

SNX

Swiss-Norwegian Foundation for Research with X-Rays

Report 2020

Contents

General Remarks.....	3
Introduction	4
Scientific highlights	5
Scientific output Impact Factors	12
Scientific output Research Areas	14
Publication list 2020.....	15
Summary of the works.....	25

General Remarks

The year 2020 is the seventeenth year of the SNX Foundation.

The accounting is supervised by OPTIMA COMPTA, in Seyssinet-Pariset, in Isère, for the two French associations, and by BfB Fidam Fiduciaire in Renens VD for the SNX Foundation. AUDICT FIDUCIAIRE in Lausanne audits the accounts.

These legal frameworks contribute to the fruitful scientific collaborations and successful research performed at the Swiss Norwegian Beam Lines at ESRF.

The activities of the SNX Foundation are carried out at the European Synchrotron Radiation Facility (ESRF) in Grenoble and comprise the operation and up-grade of two beam line branches, called the Swiss-Norwegian Beam Lines (SNBL).

Introduction

This report covers the 2020 period. After the impressive and successful startup of the new ESRF- Extremely Brilliant Source (EBS) in 2019, the imposed lockdown by the French government in spring 2020 severely disrupted the ESRF-EBS restart planning. Remarkably, regardless the delays due to the global pandemic all SNBL objectives have been reached in 2020. The ESRF has indeed re-started its new EBS in 2020 and opened it up for the beamlines. The SNBL has been preparing since 2017 for this following a plan outlined in the “SNBL 2019-2020 and beyond” document. This document was supported by the Swiss and Norwegian users, their respective steering committees and approved by the SNX Council. This document was sent out by the Paul Scherrer Institute (PSI) for international review and received excellent evaluations. The ESRF beamline review panel composed by international experts strongly endorsed the project in 2019. The document was also handed over in 2018 to the funding agencies in both Norway and Switzerland (Research Council of Norway (RCN) and State Secretariat for Education research and Innovation (SERI)). For 2020 this plan incorporates the completion of the phase 1 installation works, the commissioning with EBS and the restart of the user program.

- 1)** All installation works on both beamlines were indeed finished in time for the EBS restart
- 2)** Both beamlines were successfully fully commissioned with the new ESRF EBS source and all design parameters were reached. The now proven astounding performances in terms of accuracy, precision, reproducibility and stability of the beamlines are according to phase 1 specifications.
- 3)** The user program was successfully and reliably restarted on both beamlines
- 4)** Moreover, the year was finished with an all-time record of 142 publications using SNBL data, including one in Science and one Nature. 10% of SNBL publications has an impact factor above 10 and 45% above 4.

From the organizational perspective, we highlight that SNBL has made a smooth transition into a new contract period between the Ecole polytechnique fédérale de Lausanne - EPFL (new Swiss partner) and the Norwegian University of Science and Technology – NTNU (continuous Norwegian partner) to successfully serve its user base in 2021. Moreover, SNBL is ready to implement the phase 2 upgrades for which funding has been received from the Research Council of Norway and the Swiss National Science Foundation (R'equip grant 206021_189629).

Scientific highlights



ESRF HIGHLIGHTS 2020



PROBING CATALYST ACTIVE SITES DURING CARBON DIOXIDE HYDROGENATION TO METHANOL

The use of carbon dioxide instead of carbon monoxide for the synthesis of methanol, which is one of the most important reactants in the chemical industry, is receiving great academic and industrial attention. Here, carbon dioxide hydrogenation mechanisms and copper-zinc active phases are revisited using high-pressure *operando* XAS and SSITKA-FTIR techniques.

Chemical valorisation of carbon dioxide via thermo-catalytic hydrogenation into methanol, which is one of the most important basic molecules of the chemical industry used for the synthesis of plastics, solvents and fuels, is currently receiving great attention due to the increased global energy demand and the need to decrease the carbon footprint on the environment. For this process, a commercial copper-zinc-alumina (CZA) catalyst possessing high activity is commonly studied. The copper-zinc oxide is a unique system and prototype heterogeneous material, which has been actively investigated for decades [1-3]. Despite these efforts, driven by both academia and industry, structure-performance relations remain elusive. Multiple research groups ascribe the active sites to completely different chemical and structural centres, which triggers a debate about the role of copper-zinc alloy [4-5]. Most studies are based on experiments under *ex-situ* and *in-situ* conditions (typically vacuum and low temperature) that are far away from the real catalytic experiment (>15 bar; 513-553 K).

Hence, even a simple comparison and systematisation of the existing experimental data is a rather complicated challenge.

To address this challenge, *operando* characterisation of the catalyst and the process under relevant catalytic conditions of carbon dioxide hydrogenation was performed. Using a state-of-the-art steady-state isotope labeling experiment coupled with infrared spectroscopy (SSITKA-FTIR), together with time-resolved X-ray absorption spectroscopy (XAS), X-ray diffraction (XRD) measured at beamline BM31, and *ab-initio* modelling, it was possible to identify the reaction intermediates, the pathways of their formation, and transformations of the active sites in the copper-zinc oxide catalyst.

By varying the reduction temperature and partial pressures of hydrogen and carbon dioxide during pre-treatment steps, it was possible to tune the content of copper-zinc alloy in the catalyst. CZA materials, containing significantly different amounts of reduced zinc, possess

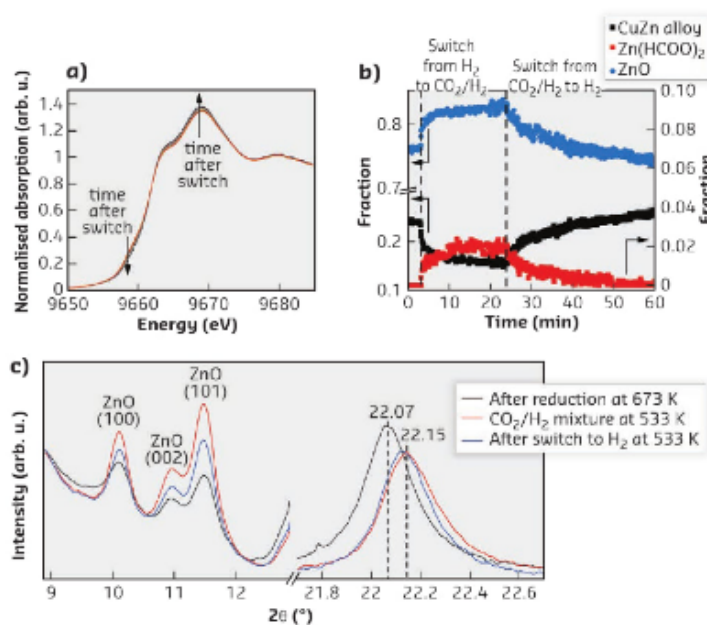


Fig. 121: **a)** Zn K-edge XANES spectra of copper-zinc oxide catalyst collected after the switch from hydrogen to CO₂/H₂ mixture. **b)** Results of PCA analysis of XANES spectra as a function of time after the switch from hydrogen to CO₂/H₂ mixture and back at 533 K and 15 bar over CZA catalyst. **c)** *Operando* XRD patterns ($\lambda = 0.4975 \text{ \AA}$) of CZA catalyst.

STRUCTURE OF MATERIALS

virtually identical catalyst activity, suggesting that no correlation exists between the observed methanol productivity and the amount of copper-zinc alloy in the system. During transient experiments by switching different gas compositions (from hydrogen to CO₂/H₂ mixture and back), it was found that copper-zinc alloy, which for a long time was considered the active site for methanol synthesis, is only stable under a highly reductive atmosphere (**Figure 121**). However, in the presence of carbon dioxide, this phase undergoes oxidation with the formation of zinc oxide and zinc formate. Combining this

finding with results obtained from the time-resolved isotope labeling experiment coupled with infrared spectroscopy, it was revealed that carbon dioxide hydrogenation to methanol occurs via a zinc formate intermediate route.

Ultimately, the role of copper-zinc alloy formation and its decomposition in forming the active interface represents a novel paradigm in this much-researched system. It can be considered as an exemplar model for structural changes in multicomponent materials and catalysts that occur during reaction.

PRINCIPAL PUBLICATION AND AUTHORS

The unique interplay between copper and zinc during catalytic carbon dioxide hydrogenation to methanol.
M. Zabilskiy (a), V.L. Sushkevich (a),

D. Palagin (a), M.A. Newton (b),
F. Krumeich (b) and J.A. van Bokhoven (a,b),
Nat. Commun. **11**, 2409 (2020); <https://doi.org/10.1038/s41467-020-16342-1>.

(a) Paul Scherrer Institute, Villigen (Switzerland)
(b) Institute for Chemical and Bioengineering, ETH Zurich (Switzerland)

REFERENCES

- [1] M. Behrens *et al.*, *Science* **336**, 893-897 (2012).
- [2] S. Kuld *et al.*, *Science* **352**, 969-974 (2016).
- [3] S. Kattel *et al.*, *Science* **355**, 1296-1299 (2017).
- [4] J. Nakamura *et al.*, *Science* **357**, eaan8074 (2017).
- [5] S. Kattel *et al.*, *Science* **357**, eaan8210 (2017).

DEGRADATION OF $\text{LaFe}_{1-x}\text{Pd}_x\text{O}_{3\pm\delta}$ PEROVSKITE-TYPE OXIDES IN BASIFIED AQUEOUS ETHANOL

Materials used for the generation of energy and chemical products often have to function in solvents that contain other chemicals. Here, an aqueous ethanol solvent, when combined with a base, causes a variety of degradative changes to a perovskite catalyst under mild conditions and even before any catalytic chemistry is considered.

Perovskites are a much-researched class of materials for areas including catalysis [1], electro-catalysis [2] and solar applications [3]. Often, in these applications, they may be required to operate in contact with a liquid of non-neutral pH. For instance, in carbon-carbon coupling catalysis, where perovskite-type oxides have been shown to be active and selective materials [4], basic compounds are required to be present in excess. Moreover, the pharmaceutical industry, where carbon-carbon

coupling catalysis is an essential foundation, has formulated guides regarding preferred solvent systems; among which are mixtures of primary alcohols and water [5]. There is significant interest in understanding how some of these solvents, and the adjuncts that must be added to them to facilitate the desired chemistry, interact with catalytic materials, in the current case a $\text{LaFe}_{1-x}\text{Pd}_x\text{O}_{3\pm\delta}$ (where $x = 0.1$) perovskite-type oxide.

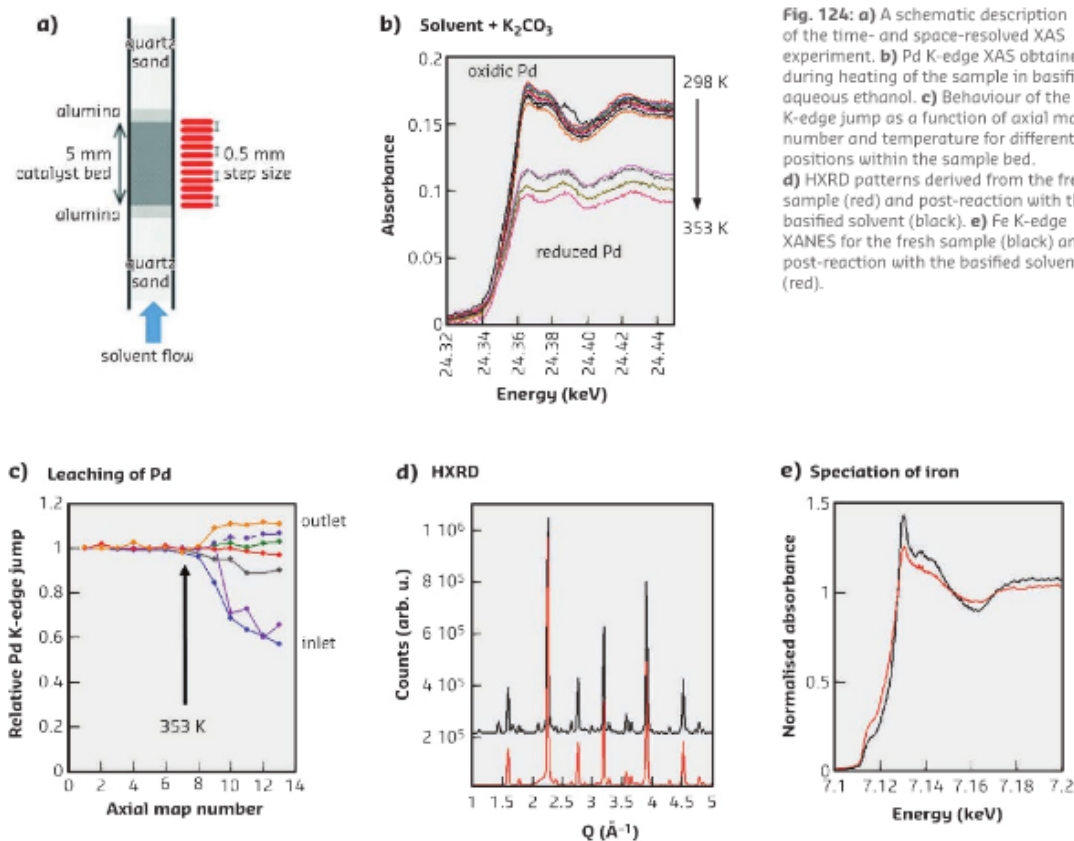


Fig. 124: a) A schematic description of the time- and space-resolved XAS experiment. b) Pd K-edge XAS obtained during heating of the sample in basified aqueous ethanol. c) Behaviour of the Pd K-edge jump as a function of axial map number and temperature for different positions within the sample bed. d) HXRD patterns derived from the fresh sample (red) and post-reaction with the basified solvent (black). e) Fe K-edge XANES for the fresh sample (black) and post-reaction with the basified solvent (red).

To follow the behaviour of the Pd component of this material in both time and space (axially along the catalyst bed), a single pass plug-flow reactor was used at **BM31**. **Figure 124a** schematically illustrates the experiment. The sample bed is heated to 353 K under the solvent flow while Pd K-edge XAS is continuously collected at 10 axial locations along the 5 mm-long bed, building up axial maps of the Pd speciation. **Figure 124b** shows typical Pd K-edge spectra that reveal two significant aspects of the behaviour of Pd occurring only in the presence of the base (K_2CO_3).

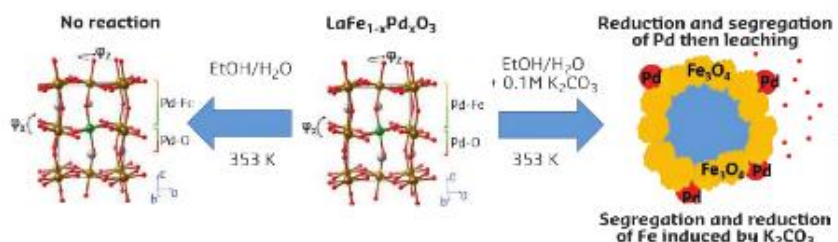
Pd K-edge XAS shows that the Pd, which initially resides in an oxidised form within the perovskite-type material, is subject to a segregative reduction to yield Pd^0 nanoparticles at 353 K. However, since the magnitude of the Pd K-edge jump itself also decreases along with reduction, some Pd is also mobilised. As **Figure 124c** shows, this occurs to varying degrees within the catalyst bed. Towards the reactor inlet, Pd is most efficiently stripped, whereas at the outlet, the intensity of the edge jump grows slightly. This shows that re-deposition also occurs along

the axial dimension, alongside the processes that cause Pd solubilisation and transport. In the absence of the base, none of these changes in the nature of Pd are observed to occur.

Pd K-edge XAS, however, cannot elucidate what may be happening in the rest of the material. Therefore, *ex-situ* high-energy X-ray scattering on **ID15A** and fluorescence Fe K-edge XANES on **BM28** was performed to investigate the other major components of the perovskite sample. Fe K-edge XANES (**Figure 124e**) shows that, along with the reduction and solubilisation of Pd, a significant proportion of Fe^{3+} is also reduced to Fe^{2+} . The X-ray scattering data (**Figure 124d**), from which Rietveld refinement and pair distribution functions (PDF) may be derived, further reveal the very significant effects that the basified solvent has on the perovskite-type oxide. In the presence of aqueous ethanol, the pristine structure of the perovskite remains intact (**Figure 125**). However, in the presence of the base, this structure is largely destroyed. What remains is composed of a shell of predominantly Fe_2O_3 , upon which the Pd that has not been solubilised remains in the form of

STRUCTURE OF MATERIALS

Fig. 125: Schematic description of how the $\text{LaFe}_{1-x}\text{Pd}_x\text{O}_3$ catalyst behaves as a result of heating in aqueous ethanol and in basified aqueous ethanol, as determined through the combined use of Pd and Fe K-edge XAS and HXRD/PDF methods.



reduced Pd nanoparticles, around a core of the starting structure.

In summary, the base can be a potent agent for leaching of palladium and the integrity of

this type of functional materials cannot be guaranteed in the presence of some of the species that are required under the typical operation conditions of the material, for example, for carbon-carbon coupling chemistry.

PRINCIPAL PUBLICATION AND AUTHORS

Pd-LaFeO₃ catalysts in aqueous ethanol: Pd reduction, leaching, and structural transformations in the presence of a base. S. Checchia (a), C.J. Mulligan (b), H. Emerich (a), I. Aïxneit (c), F. Krumeich (d),

M. Di Michiel (a), P.B.J. Thompson (a), K.K. Hii (b), D. Ferri (c) and M.A. Newton (d), *ACS Catal.* **10**, 3933-3944, (2020); <https://doi.org/10.1021/acscatal.9b04869>. (a) ESRF

(b) Department of Chemistry, Imperial College London (UK)
(c) Paul Scherrer Institut, Villigen (Switzerland)
(d) ETH Zurich (Switzerland)

REFERENCES

- [1] S. Royer *et al.*, *Chem. Rev.* **114**, 10292-10368 (2014).
- [2] F. Cheng & J. Chen, *Chem. Soc. Rev.* **41**, 2172-2192 (2012).
- [3] M.A. Green *et al.*, *Nat. Photonics*, **8**, 506-514 (2014).
- [4] S. Andrews *et al.*, *Adv. Synth. Catal.* **347**, 647-654 (2005).
- [5] D. Prat *et al.*, *Green Chem.* **16**, 4546 (2014).

SIMILAR STRUCTURAL TRANSITIONS MAY RESULT IN DRASTICALLY DIFFERENT ELECTROCHEMICAL SIGNATURES

The sodium deintercalation mechanism in two cathode materials for Na-ion batteries with a close composition ($\text{Na}_{3+x}\text{Mn}_x\text{V}_{2-x}(\text{PO}_4)_3$, $x = 0.8$ and $x = 1.0$) was studied using *operando* synchrotron X-ray powder diffraction (SXRPD). The study revealed how subtle variations in phase transformation behaviour result in drastically different electrochemical patterns of battery materials.

Na-ion batteries have recently regained great interest due to several cost, safety, and maintenance advantages as compared to widely used Li-ion and lead-acid batteries. Among various cathode materials, NASICON-type $\text{Na}_3\text{V}_2(\text{PO}_4)_3$ exhibits extremely long cyclic stability and an outstanding ability to operate at high (dis)charge rates. To improve the energy density of $\text{Na}_3\text{V}_2(\text{PO}_4)_3$, vanadium substitution by cheaper manganese was implemented. A remarkable diversity of redox couples attained

by vanadium ($\text{V}^{3+}/\text{V}^{4+}$, $\text{V}^{4+}/\text{V}^{5+}$) and manganese ($\text{Mn}^{2+}/\text{Mn}^{3+}$, $\text{Mn}^{3+}/\text{Mn}^{4+}$) at high operating potentials in NASICON-type compounds makes it feasible to utilise both transition metals in one material to improve its cost-effectiveness.

It is essential that manganese substitution incrementally changes both electrochemical signatures and the phase transformation behaviour of $\text{Na}_{3+x}\text{Mn}_x\text{V}_{2-x}(\text{PO}_4)_3$ materials. To link electrochemical features with the phase

transformations in $\text{Na}_{3+x}\text{Mn}_x\text{V}_{2-x}(\text{PO}_4)_3$ samples, *operando* high-resolution synchrotron X-ray powder diffraction (SXRPD) experiments were carried out at beamline **BM01** ($\lambda = 0.68987 \text{ \AA}$, 2D Detector Pilatus 2M, transmission mode) using an electrochemical cell with sapphire windows (**Figure 136**) [1].

Single-crystal sapphire X-ray windows provide excellent signal-to-noise ratio, proper electrochemical contact because of the constant pressure between the electrodes, and perfect electrochemical stability at high potentials due to the inert and non-conductive nature of sapphire. The design of the cell allows the simultaneous or sequential application of diffraction and spectroscopic techniques. It is particularly important to mention that this cell design allows for fluorescence detection at the outlet as well as at the inlet side of the cell. Different materials can be studied simultaneously using periodically repeating measurements with multiple cell-positioning holders.

Two $\text{Na}_{3+x}\text{Mn}_x\text{V}_{2-x}(\text{PO}_4)_3$ materials with $x = 0.8$ and 1.0 were used in this study.

The electrochemical behaviour of these samples is different (**Figure 137a**). Sodium extraction from $\text{Na}_x\text{MnV}(\text{PO}_4)_3$ proceeds via two steps in the 2.5-3.8 V voltage window, with one sloping and one flat plateau at ~ 3.4 and 3.6 V, which implies single-phase and biphasic deintercalation mechanisms, respectively [2]. Contrarily, the charging curve of $\text{Na}_{3.8}\text{Mn}_{0.8}\text{V}_{1.2}(\text{PO}_4)_3$ is wholly sloped without evident signatures of biphasic transition. *Operando* SXRPD patterns (**Figure 137b**), recorded during the charge of both electrochemical cells, show that at the beginning, Na^+ extraction from the initial $\text{Na}_{3+x}\text{Mn}_x\text{V}_{2-x}(\text{PO}_4)_3$ leads to " $\text{Na}_3\text{Mn}_x\text{V}_{2-x}(\text{PO}_4)_3$ " via reflection-shifting by a single-phase mechanism, followed by a biphasic reaction until the " $\text{Na}_{1+x}\text{Mn}_x\text{V}_{2-x}(\text{PO}_4)_3$ " composition is reached at 3.8 V.

Utilisation of highly resolving synchrotron radiation allows to clearly observe that for the case of $x = 0.8$ at approximately 50% state of charge, the " $\text{Na}_3\text{Mn}_{0.8}\text{V}_{1.2}(\text{PO}_4)_3$ " reflection broadens. Concurrently, reflection of a new " $\text{Na}_2\text{Mn}_{0.8}\text{V}_{1.2}(\text{PO}_4)_3$ " phase appears and shifts to higher 2θ angles until the " $\text{Na}_{1.8}\text{Mn}_{0.8}\text{V}_{1.2}(\text{PO}_4)_3$ "

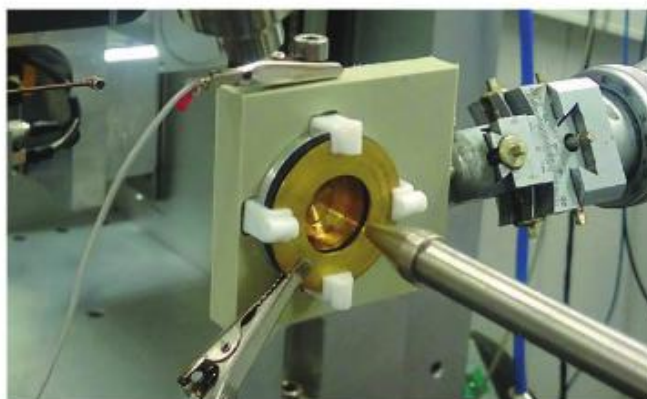
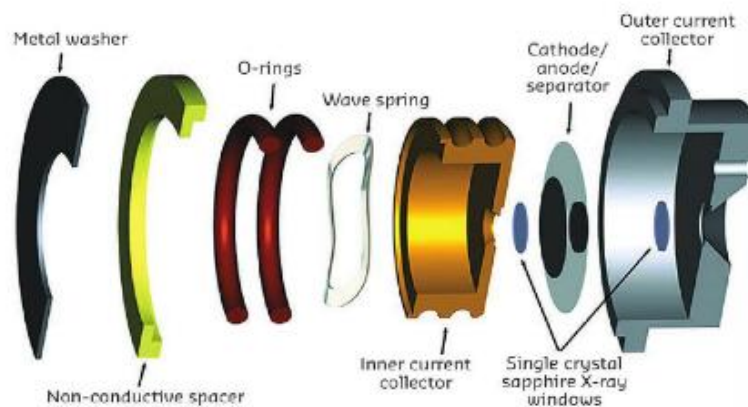


Fig. 136: Exterior and design of the electrochemical cell for *operando* X-ray measurements [1].

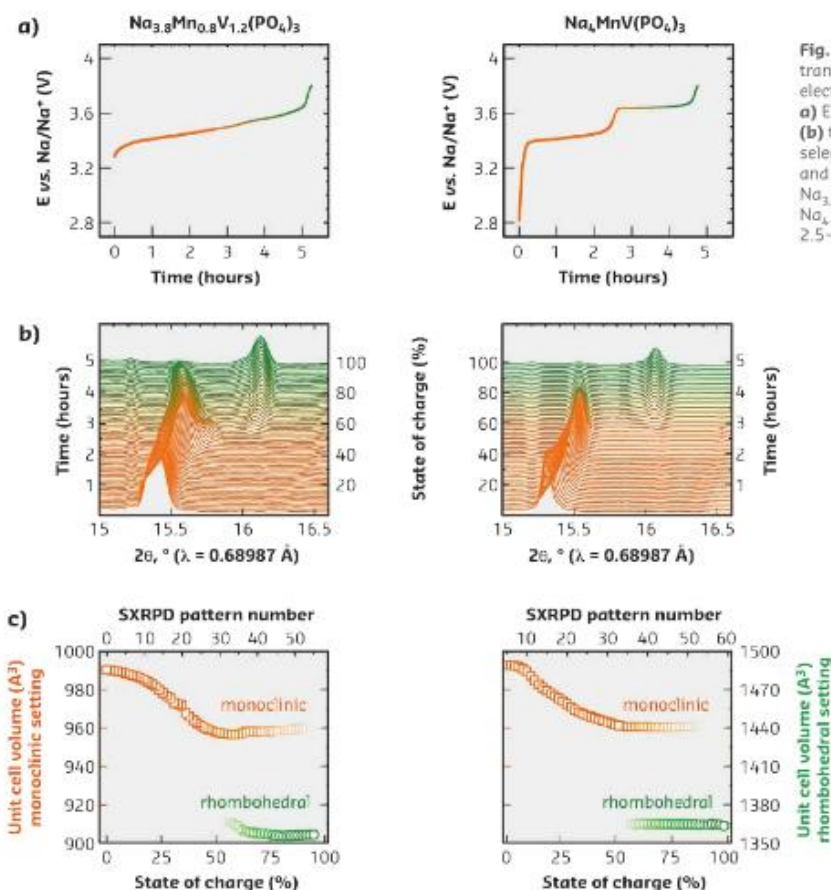


Fig. 137: Similar structural transitions may result in different electrochemical signatures. **(a)** Electrochemical charge curves, **(b)** transformations of the selected region of SXRPD patterns, and **(c)** unit cell parameters of $\text{Na}_{3.8-x}\text{Mn}_{0.8}\text{V}_{1.2}(\text{PO}_4)_3$ (left) and $\text{Na}_{4-x}\text{MnV}(\text{PO}_4)_3$ (right) within 2.5–3.8 V voltage ranges.

composition is reached. Le Bail fitting indicates an ongoing alteration of the unit cell parameters of both phases present during the biphasic domain on the charge of $\text{Na}_{3.8}\text{Mn}_{0.8}\text{V}_{1.2}(\text{PO}_4)_3$ to 3.8 V, which explains the sloped shape of the E-x curve (Figures 137b-c). In the case of $\text{Na}_4\text{MnV}(\text{PO}_4)_3$, both " $\text{Na}_3\text{Mn}_x\text{V}_{2-x}(\text{PO}_4)_3$ " and " $\text{Na}_2\text{Mn}_x\text{V}_{2-x}(\text{PO}_4)_3$ " phases don't change their 2θ position, which is reflected in the flat plateau at 3.6 V in accordance to the Gibbs phase rule.

Through *operando* SXRPD, rather unusual behaviour was observed for $\text{Na}_{3.8}\text{Mn}_{0.8}\text{V}_{1.2}(\text{PO}_4)_3$ and $\text{Na}_4\text{MnV}(\text{PO}_4)_3$ compositions, which demonstrate almost identical phase transformation behaviour but, at the same time, show absolutely different types of voltage-composition curves. These observations and the results detailed herein illustrate the necessity of *operando* synchrotron diffraction experiments, since similar structural transitions may result in the different macroscopic properties.

PRINCIPAL PUBLICATION AND AUTHORS

Electrochemical Properties and Evolution of the Phase Transformation Behavior in the NASICON-type $\text{Na}_{3-x}\text{Mn}_x\text{V}_{2-x}(\text{PO}_4)_3$ ($0 \leq x \leq 1$) Cathodes for Na-ion Batteries, M.V. Zakharkin (a,b), O.A. Drozhzhin (a,b), S.V. Ryazantsev (a,b), D. Chernyshov (c,d), M.A. Kirsanova (a), I.V. Mikheev (b).

E.M. Pazhetnov (a), E.V. Antipov (a,b) and K.J. Stevenson (a), *J. Power Sources* **470**, 1-8 (2020); <https://doi.org/10.1016/j.jpowsour.2020.228231>. (a) Skolkovo Institute of Science and Technology, Moscow (Russia), (b) Lomonosov Moscow State University,

Moscow (Russia) (c) ESRF (d) Peter the Great St. Petersburg Polytechnic University, Saint-Petersburg (Russia)

REFERENCES

- [1] O.A. Drozhzhin et al., *J. Synchrotron Radiat.* **25**, 468-472 (2018).
- [2] M.V. Zakharkin et al., *ACS Appl. Energy Mater.* **1**, 5842-5846 (2018).

Scientific output Impact Factors

142 peer reviewed papers were published in 2020 containing data from SNBL. Two papers were published in Science and Nature. 10% of the SNBL publications were published in journals with an impact factor above 10 and 45% above impact factor 4. See below the full distribution of papers per journal in 2020 and their impact factor.

Journal	Impact Factor	Publications in 2020
CHEMICAL SOCIETY REVIEWS	42.846	1
NATURE	42.779	1
SCIENCE	41.846	1
JOURNAL OF THE AMERICAN CHEMICAL SOCIETY	14.612	1
ACS NANO	14.588	1
ANGEWANDTE CHEMIE-INTERNATIONAL EDITION	12.959	3
ACS CATALYSIS	12.35	4
NATURE COMMUNICATIONS	12.121	2
JOURNAL OF MATERIALS CHEMISTRY A	11.301	1
CHEMISTRY OF MATERIALS	9.567	6
GREEN CHEMISTRY	9.48	1
NPJ 2D MATERIALS AND APPLICATIONS	9.324	1
ACS APPLIED MATERIALS & INTERFACES	8.758	2
CEMENT AND CONCRETE RESEARCH	8.328	1
JOURNAL OF POWER SOURCES	8.247	1
NANO RESEARCH	8.183	1
ACTA MATERIALIA	7.656	2
NANOSCALE	6.895	3
FOOD CHEMISTRY	6.306	1
CHEMICAL COMMUNICATIONS	5.996	1
CATALYSIS TODAY	5.825	2
CATALYSIS SCIENCE & TECHNOLOGY	5.721	4
CHEMISTRY-A EUROPEAN JOURNAL	4.857	4
CHEMCATCHEM	4.853	1
INORGANIC CHEMISTRY	4.825	4
COMMUNICATIONS PHYSICS	4.684	1
JOURNAL OF ALLOYS AND COMPOUNDS	4.65	2
MICROPOROUS AND MESOPOROUS MATERIALS	4.551	2
ACS APPLIED ENERGY MATERIALS	4.473	1
PHARMACEUTICS	4.421	1
NANOMATERIALS	4.324	2
JOURNAL OF PHYSICAL CHEMISTRY C	4.189	6
DALTON TRANSACTIONS	4.174	2
CRYSTAL GROWTH & DESIGN	4.089	1
SCIENTIFIC REPORTS	3.998	1
ORGANOMETALLICS	3.804	1

PHYSICAL REVIEW B	3.575	2
INDUSTRIAL & ENGINEERING CHEMISTRY RESEARCH	3.573	1
JOURNAL OF THE AMERICAN CERAMIC SOCIETY	3.502	1
PHYSICAL CHEMISTRY CHEMICAL PHYSICS	3.43	6
NEW JOURNAL OF CHEMISTRY	3.288	2
MOLECULES	3.267	1
SPECTROCHIMICA ACTA PART A-MOLECULAR AND BIOMOLECULAR	3.232	1
APPLIED ORGANOMETALLIC CHEMISTRY	3.14	1
CHEMMEDCHEM	3.124	1
RSC ADVANCES	3.119	1
CRYSTENGCOMM	3.117	2
MATERIALS	3.057	1
JOURNAL OF APPLIED CRYSTALLOGRAPHY	2.995	3
APPLIED GEOCHEMISTRY	2.903	1
PROCESSES	2.753	1
JOURNAL OF SOLID STATE CHEMISTRY	2.726	1
JOURNAL OF MAGNETISM AND MAGNETIC MATERIALS	2.717	2
JOURNAL OF PHYSICS-CONDENSED MATTER	2.705	1
ENERGIES	2.702	3
EUROPEAN JOURNAL OF INORGANIC CHEMISTRY	2.529	1
SOLID STATE SCIENCES	2.434	1
TOPICS IN CATALYSIS	2.406	1
CRYSTALS	2.404	2
JOURNAL OF SYNCHROTRON RADIATION	2.251	1
RADIATION PHYSICS AND CHEMISTRY	2.226	1
JOURNAL OF VACUUM SCIENCE & TECHNOLOGY A	2.166	1
METALS	2.117	1
ACTA CRYSTALLOGRAPHICA SECTION B-STRUCTURAL SCIENCE	2.048	1
JOURNAL OF SOL-GEL SCIENCE AND TECHNOLOGY	2.008	1
ARCHAEOMETRY	1.519	1
CHIMIA	1.478	1
ZEITSCHRIFT FUR ANORGANISCHE UND ALLGEMEINE CHEMIE	1.24	2
RUSSIAN JOURNAL OF COORDINATION CHEMISTRY	0.973	1
ZEITSCHRIFT FUR NATURFORSCHUNG SECTION B-A JOURNAL OF	0.839	1
CRYSTALLOGRAPHY REPORTS	0.661	1

Scientific output Research Areas

All the SNBL papers in 2020 were also classified by research area. It's clear SNBL has strong a portfolio in chemistry and materials science followed by physics and crystallography. See below the full distribution per Research Area.

Research area	Number of publications in 2020
CHEMISTRY, PHYSICAL	45
MATERIALS SCIENCE, MULTIDISCIPLINARY	44
CHEMISTRY, MULTIDISCIPLINARY	32
NANOSCIENCE & NANOTECHNOLOGY	19
CHEMISTRY, INORGANIC & NUCLEAR	17
PHYSICS, APPLIED	11
CRYSTALLOGRAPHY	10
PHYSICS, CONDENSED MATTER	8
CHEMISTRY, APPLIED	7
PHYSICS, ATOMIC, MOLECULAR & CHEMICAL	7
ENERGY & FUELS	6
METALLURGY & METALLURGICAL ENGINEERING	6
ENGINEERING, CHEMICAL	4
CHEMISTRY, ORGANIC	2
MATERIALS SCIENCE, CERAMICS	2
PHARMACOLOGY & PHARMACY	2
ARCHAEOLOGY	1
BIOCHEMISTRY & MOLECULAR BIOLOGY	1
CHEMISTRY, ANALYTICAL	1
CHEMISTRY, MEDICINAL	1
CONSTRUCTION & BUILDING TECHNOLOGY	1
ELECTROCHEMISTRY	1
FOOD SCIENCE & TECHNOLOGY	1
GEOCHEMISTRY & GEOPHYSICS	1
GEOSCIENCES, MULTIDISCIPLINARY	1
GREEN & SUSTAINABLE SCIENCE & TECHNOLOGY	1
INSTRUMENTS & INSTRUMENTATION	1
MATERIALS SCIENCE, COATINGS & FILMS	1
NUCLEAR SCIENCE & TECHNOLOGY	1
NUTRITION & DIETETICS	1
OPTICS	1
PHYSICS, MULTIDISCIPLINARY	1
SPECTROSCOPY	1

Publication list 2020

- 1 Agote-Aran, M., Kroner, A.B., Wragg, D.S., Slawinski, W.A., Briceno, M., Islam, H.U., Sazanovich, I.V., Rivas, M.E., Smith, A.W.J., Collier, P., Lezcano-Gonzalez, I., Beale, A.M. Understanding the Deactivation Phenomena of Small-Pore Mo/H-SSZ-13 during Methane Dehydroaromatisation Molecules, 25, 5048, 2020
- 2 Ahoba-Sam, C., Borfecchia, E., Lazzarini, A., Bugaev, A., Adamu Isah, A., Taoufik, M., Bordiga, S., Olsbye, U. On the conversion of CO₂ to value added products over composite PdZn and H-ZSM-5 catalysts: excess Zn over Pd, a compromise or a penalty? Catal. Sci. Technol., 10, 4373-4385, 2020
- 3 Alme, E., Törnroos, K.W., Gjertsen, B.T., Bjørsvik, H-R. Synthesis of N-Aryl- and N-alkyl-Substituted Imidazolium Silver Complexes: Cytotoxic Screening by Using Human Cell Lines Modelling Acute Myeloid Leukaemia ChemMedChem., 15, 1509-1514, 2020
- 4 Arstad, B., Blom, R., Hakonsen, S.F., Pierchala, J., Cobden, P., Lundvall, F., Kalantzopoulos, G., Wragg, D., Fjellvåg, H., Sjøstad, O. Synthesis and evaluation of K-promoted Co₃-xMg_xAl-oxides as solid CO₂ sorbents in the sorption-enhanced water-gas shift (SEWGS) Ind. Eng. Chem. Res., 2020
- 5 Asgari, M., Kochetygov, I., Abedini, H., Queen, W.L. Large anisotropic negative thermal expansion in Cu-TDPAT metal-organic framework: A combined in situ X-ray diffraction and DRIFTS study Nano Res., 2020
- 6 Asgari, M., Semino, R., Schouwink, A.P., Kochetygov, I., Tarver, J., Trukhina, O., Krishna, R., Brown, M.C., Ceriotti, M., Queen, L.W. Understanding how ligand functionalization influences CO₂ and N₂ adsorption in a sodalite MOF Chem. Mater., 32, 4, 1526-1536, 2020
- 7 Bakken, K., Blichfeld, A.B., Chernyshov, D., Grande, T., Glaum, J., Einarsrud, M-A. Mechanisms for texture in BaTiO₃ thin films from aqueous chemical solution deposition J. Sol-Gel Sci. Technol., 95, 562-572, 2020
- 8 Balaghi, E.S., Triana, A.C., Patzke, R.G. Molybdenum-Doped Manganese Oxide as a Highly Efficient and Economical Water Oxidation Catalyst ACS Catal., 10, 2074-2087, 2020
- 9 Bernal, F.L.M., Lundvall, F., Kumar, S., Hansen, P-A., Wragg, D.S., Løvvik, O.M., Fjellvåg, H. The Jahn-Teller active fluoroperovskites: thermo- and magneto optical correlations as function of the A-site Cond. Mat. Sci., 2020
- 10 Bernard, E., Jenni, A., Fisch, M., Grolimund, D., Mäder, U. Micro-X-ray diffraction and chemical mapping of aged interfaces between cement pastes and Opalinus Clay J. Appl. Geochem., 115, 104538, 2020
- 11 Blichfeld, A.B., Bakken, K., Chernyshov, D., Glaum, J., Grande, T., Einarsrud, M-A. Experimental setup for high-temperature in situ studies of crystallization of thin films with atmosphere control J. Synchrotron Rad., 27, 1209-1217, 2020
- 12 Bosak, A., Dideikin, A., Dubois, M., Ivankov, O., Lychagin, E., Muzychka, A., Nekhaev, G., Nesvizhevsky, V., Nezvanov, A., Schweins, R., Strelkov, A., Vul', A., Zhernenkov, K. Fluorination of Diamond Nanoparticles in Slow Neutron Reflectors Does Not Destroy Their Crystalline Cores and Clustering While Decreasing Neutron Losses Materials, 13, 3337, 2020
- 13 Bosak, A., Svitlyk, V., Arakcheeva, A., Burkovsky, R., Dyadkin, V., Roleder, K., Chernyshov, D. Incommensurate crystal structure of PbHfO₃ Acta Cryst., B76, 7-12, 2020
- 14 Brighi, M., Murgia, F., Cerny, R. Closo-Hydroborate Sodium Salts as an Emerging Class of Room-Temperature Solid Electrolytes Cell Rep. Phys. Science 1, 100217, 2020

- 15 Buan, M.E.M., Cognigni, A., Walmsley, J.S., Muthuswamy, N., Rønning, M. Active sites for the oxygen reduction reaction in nitrogen-doped carbon nanofibers *Catalysis Today*, in press, 2020
- 16 Bugaev, A.L., Usoltsev, O.A., Guda, A.A., Lomachenko, K.A., Brunelli, M., Groppo, E., Pellegrini, R., Soldatov, A., van Bokhoven, J.A. Hydrogenation of ethylene over palladium: Evolution of the catalyst structure by operando synchrotron-based techniques *Faraday Discuss.*, 2020
- 17 Bugaev, A.L., Zabilskiy, M., Skorynina, A.A., Usoltsev, O.A., Soldatov, A.V., van Bokhoven, J.A. In situ formation of surface and bulk oxides in small palladium nanoparticles *Chem. Commun.*, 2020
- 18 Buikin, P.A., Rudenko, A. Yu., Ilyukhin, A.B., Simonenko, N.P., Yorov, Kh. E., Kotov, V. Yu. Bromobismuthates of 1, 1'-(1, N-Alkanediyl) bis (picolines): Synthesis, Thermal Stability, Crystal Structures, and Optical Properties *Russ. J. Coord. Chem.*, 46, 111-118, 2020
- 19 Buol, X., Robeyns, K., Garrido, C.C., Tumanov, N., Collard, L., Wouters, J., Leysens, T. Improving Nefiracetam Dissolution and Solubility Behavior Using a Cocrystallization Approach *Pharmaceutics*, 12(7), 653, 2020
- 20 Cairns, A.B., Catafesta, J., Hermet, P., Rouquette, J., Levelut, C., Maurin, D., Van der Lee, A., Dmitriev, V., Bantignies, J-L., Goddwin, A.L., Haines, J. Effect of Extra-Framework Cations on Negative Linear Compressibility and High-Pressure Phase Transitions: A Study of $KCd[Ag(CN)_2]_3$ *J. Phys. Chem.*, 124, 12, 6896-6906, 2020
- 21 Castro-Fernández, P., Blanco, M.V., Verel, R., Willinger, E., Fedorov, A., Abdala, P.M., Müller, C.R. Atomic-Scale Insight into the Structure of Metastable γ -Ga₂O₃ Nanocrystals and their Thermally-Driven Transformation to β -Ga₂O₃ *J. phys. Chem. C*, 2020
- 22 Cerny, R., Brighi, M., Murgia, F. The Crystal Chemistry of Inorganic Hydroborates *Chemistry*, 2(4), 805-826, 2020
- 23 Checchia, S., Mulligan, C.J., Emerich, H., Alxneit, I., Krumeich, F., Di Michiel, M., Thompson, P.B.J., Hii, K.K., Ferri, D., Newton, M.A. Pd-LaFeO₃ catalysts in aqueous ethanol: Pd reduction, leaching, and structural transformations in the presence of a base *ACS Catal.*, 10, 6, 3933-3944, 2020
- 24 Cherednichenko, K.A., Mukhanov, V.A., Wang, Z., Oganov, A.R., Kalinko, A., Dovgaliuk, I., Solozhenko, V.L. Discovery of new boron-rich chalcogenides: orthorhombic B₆X (X= S, Se) *Sci. Rep.*, 10, 9277, 2020
- 25 Chernyshov, D., Dovgaliuk, I., Dyadkin, V., Van Beek, W. Principal Components Analysis (PCA) for Powder Diffraction Data: towards unblinded applications *Crystals*, 10(7), 581, 2020
- 26 Confalonieri, G., Fabbiani, M., Arletti, R., Quartieri, S., Di Renzo, F., Haines, J., Tabacchi, G., Fois, E., Vezzalini, G., Martra, G., Santoro, M. High-silica mordenite as scaffold for phenylacetylene polymerization: In situ high pressure investigation *J. Micro. Meso. Mater.*, 110163, 2020
- 27 Confalonieri, G., Ryzhikov, A., Arletti, R., Quartieri, S., Vezzalini, G., Isaac, C., Paillaud, J-L., Nouali, H., Daou, T.J. Structural interpretation of the energetic performances of a pure silica LTA-type zeolite *Phys. Chem. Chem. Phys.*, 22, 5178-5187, 2020
- 28 Conterosito, E., Lopresti, M., Palin, L. In Situ X-ray Diffraction Study of Xe and CO₂ Adsorption in Y Zeolite: Comparison between Rietveld and PCA-Based Analysis *Crystals*, 10(6), 483, 2020
- 29 De Maere D'Aertrycke, J-B, Morlot, J., Robeyns, K., Filinchuk, Y., Leysens, T. Exploring the solid-state phases and thermodynamics of calcium L-lactate *Food Chem.*, 325, 126884, 2020
- 30 Dejoie, C., Tamura, N. Pattern-matching indexing of Laue and monochromatic serial crystallography data for applications in materials science *J. Appl. Cryst.*, 53, 824-836, 2020

- 31 Dietzel, P.D.C., Georgiev, P.A., Frøseth, M., Johnsen, R.E., Fjellvåg, H., Blom, R. Effect of larger pore size on the sorption properties of isoreticular metal-organic frameworks with high number of open metal sites *Chem. Eur. J.*, 2020
- 32 Dovgaliuk, I., Dyadkin, V., Donckt, V.M., Filinchuk, Y., Chernyshov, D. Non-Isothermal Kinetics of Kr Adsorption by Nanoporous γ -Mg(BH₄)₂ from in Situ Synchrotron Powder Diffraction *ACS Appl. Mater. Interfaces*, 12, 6, 7710-7716, 2020
- 33 Drozhzhin, A.O., Grigoriev, V.V., Alekseeva, A.M., Ryazantsev, S.V., Tyablikov, O.A., Chernyshov, D., Abakumov, A.M., Antipov, E.V. Phase Transformations and Charge Ordering during Li+ Intercalation into Hollandite-Type TiO₂ Studied by Operando Synchrotron X-ray Powder Diffraction *Eur. J. Inorg. Chem.*, 743-748, 2020
- 34 Drozhzhin, A.O., Sobolev, V.A., Sumanov, D.V., Glazkova, S.I., Aksyonov, A.D., Grebenschikova, D.A., Tyablikov, A.O., Alekseeva, M.A., Mikheev, V.I., Dovgaliuk, I., Chernyshov, D., Stevenson, J.K., Presniakov, A.I., Abakumov, M.A., Antipov, V.E. Exploring the Origin of the Superior Electrochemical Performance of Hydrothermally Prepared Li-Rich Lithium Iron Phosphate Li_{1+ δ} Fe_{1- δ} PO₄ *J. Phys. Chem. C*, 124, 126-134, 2020
- 35 Dutta, R., Maity, A., Marsicano, A., Ceretti, M., Chernyshov, D., Bosak, A., Villesuzanne, A., Roth, G., Perversi, G., Paulus, W. Long-range oxygen ordering linked to topotactic oxygen release in Pr₂NiO_{4+ δ} fuel cell cathode material *J. Mater. Chem. A*, 8, 13987-13995, 2020
- 36 Dyadkin, V., Pattison, P., Chernyshov, D. Chirok: a post-refinement tool to analyse absolute structure *J. Appl. Cryst.*, 53, 1138-1140, 2020
- 37 El Kharbachi, A., Wind, J., Ruud, A., Høgset, A.B., Nygård, M.M., Zhang, J., Sørby, M.H., Kim, S., Cuevas, F., Orimo, S.-I., Fichtner, M., Latroche, M., Fjellvåg, H., Hauback, B.C. Pseudo-ternary LiBH₄·LiCl·P2S₅ system as structurally disordered bulk electrolyte for all-solid-state lithium batteries *Phys. Chem. Chem. Phys.*, 22, 13872-13879, 2020
- 38 Faure, S., Mille, N., Kale, S., Asensio, J.M., Marbaix, J., Farger, P., Stoian, D., Van Beek, W., Fazzini, P.-F., Soulantica, K., Chaudret, B., Carrey, J. Internal Temperature Measurements by X-ray Diffraction on Magnetic Nanoparticles Heated by a High-Frequency Magnetic Field *J. Phys. Chem.*, 2020
- 39 Feig, M., Akselrud, L., Schnelle, W., Dyadkin, V., Chernyshov, D., Ormeci, A., Simon, P., Leithe-Jasper, A., Gumeniuk, R. Crystal structure, chemical bonding, and electrical and thermal transport in Sc₅Rh₆Sn₁₈ *Dalton Trans.*, 49, 6832-6841, 2020
- 40 Fischer, N., Claeys, M. In situ characterization of Fischer–Tropsch catalysts: a review *J. of Phys. D: Appl. Phys.*, 53, 293001, 2020
- 41 Fovanna, T., Campisi, S., Villa, A., Kambolis, A., Peng, G., Rentsch, D., Kröcher, O., Nachttegaal, M., Ferri, D. Ruthenium on phosphorous-modified alumina as an effective and stable catalyst for catalytic transfer hydrogenation of furfural *RSC Adv.*, 10, 11507-11516, 2020
- 42 Gaur, A., Stehle, M., Viegaard Raun, K., Thrane, J., Degn Jensen, A., Grunwaldt, J.-D., Høj, M. Structural dynamics of an iron molybdate catalyst under redox cycling conditions studied with in situ multi edge XAS and XRD *Phys. Chem. Chem. Phys.*, 22, 11713-11723, 2020
- 43 Gorfman, S., Choe, H., Zhang, G., Zhang, N., Yokota, H., Glazer, A.M., Xie, Y., Dyadkin, V., Chernyshov, D., Ye, Z.-G. New method to measure domain-wall motion contribution to piezoelectricity: the case of PbZr_{0.65}Ti_{0.35}O₃ ferroelectric *J. Appl. Cryst.*, 53, 1039-1050, 2020

- 44 Gramm, V.K., Smets, D., Grzesiak, I., Block, T., Pöttgen, R., Suta, M., Wickleder, C., Lorenz, T., Ruschewitz, U. Eu(O₂C-CC-CO₂): An EuII Containing Anhydrous Coordination Polymer with High Stability and Negative Thermal Expansion Chem. Eur. J., 26, 1-10, 2020
- 45 Grendal, O.G., Nylund, I-E., Blichfeld, A.B., Tominaka, S., Ohara, K., Selbach, S.M., Grande, T., Einarsrud, M-A. Controlled growth of Sr_xBa_{1-x}Nb₂O₆ hopper-and cube-shaped nanostructures by hydrothermal synthesis Chem. Eur. J., 26, 9348-9355, 2020
- 46 Grinderslev, J.B., Amdisen, M.B., Jensen, T.R. Synthesis, Crystal Structures and Thermal Properties of Ammine Barium Borohydrides Inorganics, 8, 57, 2020
- 47 Grinderslev, J.B., Jepsen, L.H., Lee, Y-S., Møller, K.T., Cho, W., Cerný, R., Jensen, T.R. Structural Diversity and Trends in Properties of an Array of Hydrogen-Rich Ammonium Metal Borohydrides Inorg. Chem., 2020
- 48 Grinderslev, J.B., Lee, Y-S., Paskevicius, M., Møller, K.T., Yan, Y., Cho, Y.W., Jensen, T.R. Ammonium–Ammonia Complexes, N₂H₇⁺, in Ammonium closo-Borate Amines: Synthesis, Structure, and Properties Inorg. Chem., 59, 16, 11449-11458, 2020
- 49 Grinderslev, J.B., Ley, M.B., Lee, Y-S., Jepsen, L.H., Jørgensen, M., Cho, Y.W., Skibsted, J., Jensen, T.R. Ammine Lanthanum and Cerium Borohydrides, M(BH₄)₃·nNH₃; Trends in Synthesis, Structures, and Thermal Properties Inorg. Chem., 59, 11, 7768-7778, 2020
- 50 Hassen, S., Chebbi, H., Arfaoui, Y., Robeyns, K., Steenhaut, T., Hermans, S., Filinchuk, Y. Spectroscopic and structural studies, thermal characterization, optical properties and theoretical investigation of 2-aminobenzimidazolium tetrachlorocobaltate(II) Spectrochimica Acta Part A: Mol. Biomol. Spectro., 240, 118612, 2020
- 51 Hetzert, M., Tobeck, C., Ruschewitz, U. NaSeC₂H: A Crystalline Compound with Disordered – SeC₂H Anions Z. Anorg. Allg. Chem., 646, 1-6, 2020
- 52 Holmsen M.S.M., Nova, A., Øien-Ødegaard, S., Heyn, R.H., Tilset, M. A Highly Asymmetric Gold(III) h₃-Allyl Complex Angew. Chem. Int., 59, 1516-1520, 2020
- 53 Hölscher, J., Andersen, H.L., Saura-Múzquiz, M., Garbus, G.P., Christensen, M. Correlation between microstructure, cation distribution and magnetism in Ni_{1-x}Zn_xFe₂O₄ nanocrystallites CrystEngComm, 22, 515-524, 2020
- 54 Hölscher, J., Saura-Múzquiz, M., Ahlburg, J.V., Mørch, M., Grønseth, D., Christensen, M. Controlling structural and magnetic properties of SrFe₁₂O₁₉ nanoplatelets by synthesis route and calcination time J. Phy. D: Appl. Phys., 2020
- 55 Hosseiniamoli, H., Setiawan, A., Adesina, A.A., Kennedy, M.E., Stockenhuber, M. The stability of Pd/TS-1 and Pd/silicalite-1 for catalytic oxidation of methane – understanding the role of titanium Catal. Sci. Technol., 10, 1193-1204, 2020
- 56 Hunvik, K.W.B., Loch, P., Cavalcanti, L.P., Seljelid, K.K., Røren, P.M., Rudic, S., Wallacher, D., Kirch, A., Knudsen, K.D., Miranda, C.R., Breu, J., Bordallo, H.N., Fossum, J.O. CO₂ Capture by Nickel Hydroxide Interstratified in the Nanolayered Space of a Synthetic Clay Mineral J. Phys. Chem. C, 124, 48, 26222-26231, 2020
- 57 Jablonka, K.M., Moosavi, S.M., Asgari, M., Ireland, C., Patiny, L., Smit, B. A Data-Driven Perspective on the Colours of Metal-Organic Frameworks ChemRxiv, 2020
- 58 Jankowska-Sumara, I., Pasciak, M., Kadziolka-Gawel, M., Podgorna, M., Majchrowski, A., Roleder, K. Local properties and phase transitions in Sn doped antiferroelectric PbHfO₃ single crystal J. Phys.: Condens. Matter, 32, 435402, 2020

- 59 Jørgensen, M., Shea, T.P., Tomich, W.A., Varley, B.J., Bercx, M., Lovera, S., Cerný, R., Zhou, W., Udovic, J.T., Lavallo, V., Jensen, R.T., Wood, C.B., Stavila, V. Understanding Superionic Conductivity in Lithium and Sodium Salts of Weakly Coordinating Closo-Hexahalocarborate Anions *Chem. Mater.*, 32, 4, 1475-1487, 2020
- 60 Kalantzopoulos, N.G., Lundvall, F., Thorshaug, K., Lind, A., Vajeeston, P., Dovgaliuk, I., Arstad, B., Wragg, S.D., Fjellvåg, H. Factors Determining Microporous Material Stability in Water: The Curious Case of SAPO-37 *Chem. Mater.*, 32, 4, 1495-1505, 2020
- 61 Karve, V.V., Sun, D.T., Trukhina, O., Yang, S., Oveisi, E., Luterbacher, J., Queen, W.L. Efficient reductive amination of HMF with well dispersed Pd nanoparticles immobilized in a porous MOF/polymer composite *Green Chem.*, 22, 368-378, 2020
- 62 Khodakov, A.Y., Ordonsky, V.V., Palcic, A., Cai, M., Subramanian, V., Luo, Y., Valtchev, V., Moldovan, S., Ersen, O. Assessment of metal sintering in the copper-zeolite hybrid catalyst for direct dimethyl ether synthesis using synchrotron-based X-ray absorption and diffraction *Catal. Today*, 343, 199-205, 2020
- 63 Kiani, M., Bagherzadeh, M., Meghdadi, S., Fadaei-Tirani, F., Schenk-Joß, K., Rabiee, N. Catalytic and antibacterial properties of 3-dentate carboxamide Pd/Pt complexes obtained via a benign route *Appl. Organometal. Chem.*, e5531, 2020
- 64 Kiani, M., Bagherzadeh, M., Meghdadi, S., Rabiee, N., Abbasi, A., Schenk-Joß, K., Tahriri, M., Tayebi, L., Webster, T.J. Development of a novel carboxamide-based off-on switch fluorescence sensor: Hg²⁺, Zn²⁺ and Cd²⁺ *New J. Chem.*, 44, 11841-11852, 2020
- 65 Kirichkov, M.V., Bugaev, A.L., Skorynina, A.A., Butova, V.V., Budnyk, A.P., Guda, A.A., Trigub, A.L., Soldatov, A.V. In Situ Time-Resolved Decomposition of β -Hydride Phase in Palladium Nanoparticles Coated with Metal-Organic Framework Metals, 10(6), 810, 2020
- 66 Kiriukhina, G.V., Yakubovich, O.V., Dovgaliuk, I.N., Dimitrova, O.V., Volkov, A.S. Crystal Structure of the Potassium-Rich Analog of Manaksite K (K_{0.72} Na_{0.28}) Mn [Si₄ O₁₀] Based on the Low-Temperature Synchrotron Experiment Data *Crystallogr. Rep.*, 65, 33-39, 2020
- 67 Kirsanova, M.A., Ryazantsev, S.V., Abakumov, A.M. Anionic substitution in LiMnPO₄: The Li_{1-x}Mn_{1+x} (PO₄)_{1-y-z} (VO₄)_y (OH)_{4z} solid solutions prepared with a microwave-assisted hydrothermal method *J. of Solid State Chem.*, 286, 121294, 2020
- 68 Kirste, K.G., Laassiri, S., Hu, X., Stoian, D., Torrente-Murciano, L., Hargreaves, J.S.J., Mathisen, K. XAS investigation of silica aerogel supported cobalt rhenium catalysts for ammonia decomposition *Phys. Chem. Chem. Phys.*, Advance Article, 2020
- 69 Kirste, K., McAuley, K., Bell, T.E., Stoian, D., Laassiri, S., Daisley, A., Hargreaves, J.S.J., Mathisen, K., Torrente-Murciano, L. CO_x-free hydrogen production from ammonia—mimicking the activity of Ru catalysts with unsupported Co-Re alloys *J. Applied Cat. B: Environmental*, 119405, 2020
- 70 Klimova, N., Yefanov, O., Snigirev, A. Predicting glitches of intensity in single-crystal diamond CRLs *AIP Conference Proceedings*, 2299, 060016, 2020
- 71 Kokliukhin, A., Nikulshina, M., Mozhaev, A., Lancelot, C., Lamonier, C., Nins, N., Blanchard, P., Bugaev, A., Nikulshin, P. Bulk hydrotreating MonW₁₂-nS₂ catalysts based on SiMonW₁₂-n heteropolyacids prepared by alumina elimination method *Catal. Today*, 2020
- 72 Konevtsova, O.V., Roshal, D.S., Dmitriev, V.P., Rochal S.B. Carbon nanotube sorting due to commensurate molecular wrapping *Nanoscale*, 12, 15725-15735, 2020
- 73 Krüger, M., Liebug, S., Ruschewitz, U. K_xRb_{2-x}PdC₂: A Solid Solution of a Quaternary Acetylide with Vegard Behavior *Z. Anorg. Allg. Chem.*, 646, 570-573, 2020

- 74 Kumar, S., Fjellvåg, Ø., Olafsen, A., Fjellvåg, H. Physical properties of Ruddlesden-Popper ($n = 3$) nickelate: $\text{La}_4\text{Ni}_3\text{O}_{10}$ *J. Magnetism and Magnetic Materials*, 496, 165915, 2020
- 75 Kurdin, K.A., Kuznetsov, V.V., Sinityn, V.V., Galitskaya, E.A., Filatova, E.A., Belina, C.A., Stevenson, K.J. Synthesis and characterization of Pt-HxMoO₃ catalysts for CO-tolerant PEMFCs *Catal. Today*, 2020
- 76 Kurlov, A., Deeva, E.B., Abdala, P.M., Lebedev, D., Tsoukalou, A., Comas-Vives, A., Fedorov, A., Müller, C.R. Exploiting two-dimensional morphology of molybdenum oxycarbide to enable efficient catalytic dry reforming of methane *Nature Comm.*, 11, 4920, 2020
- 77 Kurlov, A., Huang, X., Deeva, E.B., Abdala, P.M., Fedorov, A., Müller, C.R. Molybdenum Carbide and Oxycarbide from Carbon-Supported MoO₃ Nanosheets: Phase Evolution and DRM Catalytic Activity Assessed by TEM and in situ XANES/XRD methods *Nanoscale*, 12, 13086-13094, 2020
- 78 Kuznetsov, D.A., Naeem, M.A., Kumar, P.V., Abdala, P.M., Fedorov, A., Müller, C.R. Tailoring Lattice Oxygen Binding in Ruthenium Pyrochlores to Enhance Oxygen Evolution Activity *J. Am. Chem. Soc.*, 142, 17, 7883-7888, 2020
- 79 Kvalvik, J.N., Kvamme, K.B., Almaas, K., Ruud, A., Sønsteby, H.H., Nilsen, O. LiF by atomic layer deposition—Made easy *J. Vac. Sci. Technol. A*, 38, 050401, 2020
- 80 Kvande, K., Pappas, D.K., Borfecchia, E., Lomachenko, K.A. Advanced X-ray Absorption Spectroscopy Analysis to Determine Structure-Activity Relationships for Cu-Zeolites in the Direct Conversion of Methane to Methanol *ChemCatChem.*, 12, 2385-2405, 2020
- 81 Li, X., Bianchini, F., Wind, J., Pettersen, C., Wragg, D.S., Vajeeston, P., Fjellvåg, H. Insights into Crystal Structure and Diffusion of Biphasic $\text{Na}_2\text{Zn}_2\text{TeO}_6$ *ACS Appl. Mater. Interfaces*, 12, 25, 28188-28198, 2020
- 82 Liu, H., Grendal, O.G., Skjærvø, S.L., Dalod, A.R.M., Van Beek, W., Sekkat, A., Einarsrud, M-A., Muñoz-Rojas, D. Reaction Pathway of the Hydrothermal Synthesis of AgCuO_2 from In Situ Time-Resolved X-ray Diffraction *Cryst. Growth Des.*, 20, 7, 4264-4272, 2020
- 83 Llamas Jansa, I., Friedrichs, O., Fichtner, M., Bardají, E.G., Züttel, A., Hauback, B.C. Effects of Ball Milling and TiF_3 Addition on the Dehydrogenation Temperature of $\text{Ca}(\text{BH}_4)_2$ Polymorphs *Energies*, 13, 4828, 2020
- 84 Llewellyn, A.V., Matruglio, A., Brett, D.J.L., Jarvis, R., Shearing, P.R. Using In-Situ Laboratory and Synchrotron-Based X-ray Diffraction for Lithium-Ion Batteries Characterization: A Review on Recent Developments *Condens. Matter*, 5, 75, 2020
- 85 Mantella, V., Strach, M., Frank, K., Pankhurst, J.R., Stoian, D., Gadiyar, C., Nickel, B., Buonsanti, R. Polymer Lamellae as Reaction Intermediates in the Formation of Copper Nanospheres as Evidenced by In Situ X-ray Studies *Ang. Chem. Int. Ed.*, 59, 11627-11633, 2020
- 86 Mariette, C., Trzop, E., Mevellec, J-Y., Boucekkine, A., Ghoufi, A., Maurin, G., Collet, E., Carmen Muñoz, M., Real, J.A., Toudic, B. Symmetry breakings in a metal organic framework with a confined guest *Phys. Rev. B*, 101, 134103, 2020
- 87 Marshall, K.P., Blichfeld, A.B., Skjærvø, S.L., Grendal, O.G., Van Beek, W., Selbach, S.M., Grande, T., Einarsrud, M-A. A fast, low temperature synthesis method for hexagonal YMnO_3 : Kinetics, purity, size and shape as studied by in situ X-ray diffraction *Chem. Eur. J.*, 26, 9330-9337, 2020
- 88 Martino, E., Pisoni, A., Ciric, L., Arakcheeva, A., Berger, H., Akrap, A., Putzke, C., Moll, P.J.W., Batistic, I., Tutis, E., Forró, L., Semeniuk, K. Preferential out-of-plane conduction and quasi-one-dimensional electronic states in layered 1T-TaS₂ *npj 2D Mater. Appl.*, 4, 7, 2020

- 89 Mauroy, H., Klyukin, K., Shelyapina, M.G., Keen, D.A., Thøgersen, A., Hauback, B., Sørby, M.H. Short-Range Structure of $\text{Ti}_{0.63}\text{V}_{0.27}\text{Fe}_{0.10}\text{D}_{1.73}$ from neutron total scattering and reverse Monte Carlo Modelling *Energies*, 13(8), 1947, 2020
- 90 Meyet, J., Newton, M.A., Van Bokhoven, J.A., Copéret, C. Molecular Approach to Generate Cu(II) Sites on Silica for the Selective Partial Oxidation of Methane *CHIMIA Inter. J. for Chem.*, 74, 4, 237-240(4), 2020
- 91 Naeem, A.M., Abdala, M.P., Armtlulu, A., Kim, M.S., Fedorov, A., Müller, R.C. Exsolution of Metallic Ru Nanoparticles from Defective, Fluorite-Type Solid Solutions $\text{Sm}_2\text{Ru}_x\text{Ce}_{2-x}\text{O}_7$ To Impart Stability on Dry Reforming Catalysts *ACS Catal.*, 10, 1923-1937, 2020
- 92 Naeem, A.M., Burueva, D.B., Abdala, M.P., Bushkov, N.S., Stoian, D., Bukhtiyarov, A.V., Prosvirin, I.P., Bukhtiyarov, V.I., Kovtunov, K.V., Koptyug, I.V., Fedorov, A., Müller, R.C. Deciphering the Nature of Ru Sites in Reductively Exsolved Oxides with Electronic and Geometric Metal-Support Interactions *J. Phys. Chem. C*, 124, 46, 25299-25307, 2020
- 93 Newton, A.M., Ferri, D., Mulligan, J.C., Alxneit, I., Emerich, H., Thompson, J.B.P., Hii (Mimi), K.K. In situ study of metal leaching from Pd/ Al_2O_3 induced by K_2CO_3 *Catal. Sci. Technol.*, 10, 466, 2020
- 94 Newton, A.M., Knorpp, A.J., Meyet, J., Stoian, D., Nachtegaal, M., Clark, A.H., Safonova, O.V., Emerich, H., Van Beek, W., Sushkevich, V.L., Van Bokhoven, J.A. Unwanted effects of X-rays in surface grafted copper (II) organometallics and copper exchanged zeolites, how they manifest, and what can be done about them *Phys. Chem. Chem. Phys.*, 22, 6826-6837, 2020
- 95 Newton, A.M., Knorpp, A.J., Sushkevich, V.L., Palagin, D., Van Bokhoven, J.A. Active sites and mechanisms in the direct conversion of methane to methanol using Cu in zeolitic hosts: a critical examination *Chem. Soc. Rev.*, 49, 1449-1486, 2020
- 96 Nicholson, W.C., Schwier, F.E., Shimada, K., Berger, H., Hoesch, M., Berthod, C., Monney, C. Role of a higher-dimensional interaction in stabilizing charge density waves in quasi-one-dimensional NbSe_3 revealed by angle-resolved photoemission spectroscopy *Phys. Rev. B*, 101, 045412, 2020
- 97 Nygård, M.M., Slawinski, W.A., Ek, G., Sørby, M.H., Sahlberg, M., Keen, D.A., Hauback, B.C. Local order in high-entropy alloys and associated deuterides – a total scattering and Reverse Monte Carlo study *Acta Materialia*, 199, 504-513, 2020
- 98 Nygård, M.M., Sørby, M.H., Grimenes, A.A., Hauback, B.C. The Influence of Fe on the Structure and Hydrogen Sorption Properties of Ti-V-Based Metal Hydrides *Energies*, 13(11), 2874, 2020
- 99 Ould-Amara, S., Yadav, V., Petit, E., Maurin, G., Yot, G.P., Demirci, B.U. Calcium hydrazinidoborane: Synthesis, characterization, and promises for hydrogen storage *International J. of Hydrogen Energy*, 45, 2022-2033, 2020
- 100 Ovsyannikov, V.S., Bykov, M., Medvedev, B.M., Naumov, G.P., Jesche, A., Tsirlin, A.A., Bykova, E., Chuvashova, I., Karkin, E.A., Dyadkin, V., Chernyshov, D., Dubrovinsky, S.L. A Room-Temperature Verwey-type Transition in Iron Oxide, Fe_5O_6 *Angew. Chem. Int.*, 59, 1-6, 2020
- 101 Park, J., Collins, B., Darago, L., Runcevski, T., Aubrey, M., Jiang, H.Z.H., Velasquez, E., Green, M., Goodpaster, J., Long, J.R. Magnetic Ordering via Itinerant Ferromagnetism in a Metal-Organic Framework *ChemRxiv*, 2020
- 102 Pato-Doldán, B., Rosnes, M.H., Chernyshov, D., Dietzel, P.D. Carbon dioxide induced structural phase transition in metal-organic frameworks CPO-27 *CrystEngComm.*, 22, 4353-4358, 2020

- 103 Payandeh, S., Asakura, R., Avramidou, P., Rentsch, D., Lodziana, Z., Cerny, R., Remhof, A., Battaglia, C. Nido-Borate/Closo-Borate Mixed-Anion Electrolytes for All-Solid-State Batteries *Chem. Mater.* 2020, 32, 3, 1101-1110
- 104 Periyasamy, M., Fjellvåg, O.S., Fjellvåg, H., Sjøstad, A.O. Coupling of magnetoresistance switching and glassy magnetic state at the metal-insulator transition in Ruddlesden-Popper manganate $\text{Ca}_4\text{Mn}_3\text{O}_{10}$ *J. of Magnetism and Magnetic Mat.*, 511, 166949, 2020
- 105 Periyasamy, M., Patra, L., Fjellvåg, O.S., Ravindran, P., Sørby, M.H., Kumar, S., Sjøstad, A.O., Fjellvåg, H. Electron doping of the layered nickelate $\text{La}_4\text{Ni}_3\text{O}_{10}$ by aluminum substitution: A combined experimental and DFT study *Cond. Mat. Sci.*, 2020
- 106 Perlepe, P., Oyarzabal, I., Mailman, A., Yquel, M., Platonov, M., Dovgaliuk, I., Rouzières, M., Négrier, P., Mondieig, D., Suturina, E.A., Dourges, M.-A., Bonhommeau, S., Musgrave, R.A., Pedersen, K.S., Chernyshov, D., Wilhelm, F., Rogalev, A., Mathonière, C., Clérac, R. Metal-organic magnets with large coercivity and ordering temperatures up to 242°C *Science*, 370, 587-592, 2020
- 107 Polisi, M., Vezzalini, M.G., Bonaccorsi, E., Biagioni, C., Arletti, R. High pressure behaviour of tobermorite supergroup minerals: An in situ synchrotron X-ray powder diffraction study *Cement and Concrete Research*, 138, 106249, 2020
- 108 Rasmussen, K.L., Delbey, T., Skytte, L., La Nasa, J., Colombini, M.P., Ravnsbæk, D.B., Jørgensen, B., Kjeldsen, F., Grønnow, B., Larsen, S. In the darkest hour - Analyses of a black spot on the last page of the diary of polar explorer Jørgen Brønlund (†1907) *Archaeometry*, Accepted Article, 2020
- 109 Rosnes, M.H., Pato-Doldán, B., Johnsen, R.E., Mundstock, A., Caro, J., Dietzel, P.D.C. Role of the metal cation in the dehydration of the microporous metal-organic frameworks CPO-27-M *J. Micro. Meso. Mater.*, 110503, 2020
- 110 Ruschewitz, U., Gramm, V.K., Smets, D., Grzesiak, I., Block, Th., Pöttgen, R., Suta, M., Wickleder, C., Lorenz, Th. $\text{Eu}(\text{O}_2\text{C-CC-CO}_2)$: An EuII Containing Anhydrous Coordination Polymer with High Stability and Negative Thermal Expansion *Chem. Eur. J.*, 26, 2726-2734, 2020
- 111 Ruschewitz, U., Liebig, S., Krüger, M. $\text{K}_x\text{Rb}_{2-x}\text{PdC}_2$: A Solid Solution of a Quaternary Acetylide with Vegard Behaviour *Z. anorg. allg. Chem.*, 646, 570-573, 2020
- 112 Saura-Múzquiz, M., Eikeland, A.Z., Stingaciu, M., Andersen, H.L., Granados-Miralles, C., Avdeev, M., Luzin, V., Christensen, M. Elucidating the relationship between nanoparticle morphology, nuclear/magnetic texture and magnetic performance of sintered $\text{SrFe}_{12}\text{O}_{19}$ magnets *Nanoscale*, 12, 9481-9494, 2020
- 113 Schuler, R., Norby, T., Fjellvåg, H. Defects and polaronic electron transport in Fe_2WO_6 *Phys. Chem. Chem. Phys.*, 22, 15541-15548, 2020
- 114 Serrer, M.-A., Gaur, A., Jelic, J., Weber, S., Fritsch, C., Clark, A.H., Saraçi, E., Studt, F., Grunwaldt, J.-D. Structural dynamics in Ni-Fe catalysts during CO_2 methanation – role of iron oxide clusters *Catal. Sci. Technol.*, 2020, Advance Article
- 115 Sieuw, L., Lakraychi, A.E., Rambabu, D., Robeyns, K., Jouhara, A., Borodi, G., Morari, C., Poizot, P., Vlad, A. Through-Space Charge Modulation Overriding Substituent Effect: Rise of the Redox Potential at 3.35 V in a Lithium-Phenolate Stereoelectronic Isomer *Chem. Mater.*, 32, 23, 9996-10006, 2020

- 116 Simonov, A., De Baerdemaeker, T., Boström L. B., H., Ríos Gómez, M. L., Gray, H.J., Chernyshov, D., Bosak, A., Bürgi, H-B., Goodwin, A.L. Hidden diversity of vacancy networks in Prussian blue analogues *Nature* 578, 256–260 (2020)
- 117 Skorynina, A.A., Tereshchenko, A.A., Usoltsev, O.A., Bugaev, A.L., Lomachenko, K.A., Guda, A.A., Groppo, E., Pellegrini, R., Lamberti, C., Soldatov, A.V. Time-dependent carbide phase formation in palladium nanoparticles *Rad. Phys. and Chem.*, 175, 2020
- 118 Slebarski, A., Zajdel, P., Maska, M.M., Deniszczuk, J., Fijalkowski, M. Superconductivity of Y5Rh6Sn18; Coexistence of the high temperature thermal lattice relaxation process and superconductivity *J. of Alloys and Compounds*, 819, 152959, 2020
- 119 Sørensen, D.R., Drejer, A.O., Karlsen, M.A., Nielsen, U.G., Heere, M., Senyshyn, A., Ravnsbæk, D.B. Effect of Oxygen Defects on the Structural Evolution of LiVPO4F1–yOy Cathode Materials *ACS Appl. Energy Mater.*, 2020
- 120 Steele, J.A., Solano, E., Jin, H., Prakasam, V., Braeckevelt, T., Yuan, H., Lin, Z., de Kloe, R., Wang, Q., Rogge, S.M.J., Van Speybroeck, V., Chernyshov, D., Hofkens, J., Roeffaers, M.B.J. Texture Formation in Polycrystalline Tin Films of All-Inorganic Lead Halide Perovskite *Condens. Mat. Sci.*, 2020
- 121 Steenhaut, T., Hermans, S., Filinchuk, Y. Green synthesis of a large series of bimetallic MIL-100(Fe,M) MOFs *New J. Chem.*, 44, 3847-3855, 2020
- 122 Sudan, S., Gladysiak, A., Valizadeh, B., Lee, J-H., Stylianou, K.C. Sustainable Capture of Aromatic Volatile Organic Compounds by a Pyrene-Based Metal–Organic Framework under Humid Conditions *Inorg. Chem.*, 59, 13, 9029-9036, 2020
- 123 Szpunar, I., Wachowki, S., Miruszewski, T., Dzierzgowski, K., Górnicka, K., Klimczuk, T., Sørby, H.M., Balaguer, M., Serra, M.J., Strandbakke, R., Gazda, M., Mielewczyk-Gryń, A. Electric and magnetic properties of lanthanum barium cobaltite *J. Am. Ceram. Soc.*, 103, 1809-1818, 2020
- 124 Tang, H., Wang, Z., Mamakhel, H.A.M., Dong, M., Christensen, M. Combustion assisted preparation of high coercivity SmCo hard magnet with stable single-domain size *J. of Alloys and Compounds*, 816, 152527, 2020
- 125 Tedenac, J-C., Yot, P.G., Bulanova, M., Fartushna, J., Colinet, C. Evidence of an ordered ternary phase in the section Ni–Ti5Sn3 of the ternary Ti–Ni–Sn: Crystal structure and phase stability *Solid State Sciences*, 109, 106349, 2020
- 126 Tian, Y., Maulbetsch, T., Jordan, R., Törnroos, K.W., Kunz, D. Synthesis and Reactivity of Cobalt(II) and Iridium(I) Complexes Bearing a Pentadentate N-Homoallyl-Substituted Bis(NHC) Pincer Ligand *Organometallics*, 39, 8, 1221-1229, 2020
- 127 Tsoukalou, A., Abdala, P.M., Armutlulu, A., Willinger, E., Fedorov, A., Müller, C.R. Operando X-Ray Absorption Spectroscopy Identifies Monoclinic ZrO2:In Solid Solution as the Active Phase for the Hydrogenation of CO2 to Methanol *ACS Catal.*, 2020
- 128 Usoltsev, O.A., Bugaev, A.L., Guda, A.A., Guda, A.S., Soldatov, A.V. Absorption of Hydrocarbons on Palladium Catalysts: From Simple Models Towards Machine Learning Analysis of X-ray Absorption Spectroscopy Data *Top. Catal.*, 63, 58-65, 2020
- 129 Usoltsev, O.A., Pnevskaya, A.Y., Kamyshova, E.G., Tereshchenko, A.A., Skorynina, A.A., Zhang, W., Yao, T., Bugaev, A.L., Soldatov, A.V. Dehydrogenation of Ethylene on Supported Palladium Nanoparticles: A Double View from Metal and Hydrocarbon Sides *Nanomaterials*, 10, 1643, 2020
- 130 Venkateshwarlu, S., Venkataraman, L.K., Segouin, V., Marlton, F.P., Hin, H.C., Chernyshov, D., Ren, Y., Jørgensen, M.R.V., Nayak, S., Rödel, J., Daniel, L., Pramanick, A. Large electromechanical

- strain and unconventional domain switching near phase convergence in a Pb-free ferroelectric Commun. Phys., 3, 193, 2020
- 131 Wachowski, S.L., Szpunar, I., Sørby, M.H., Mielewczyk-Gryn, A., Balaguer, M., Ghica, C., Istrate, M.C., Gazda, M., Gunnæs, A.E., Serra, J.M., Norby, T., Strandbakke, R. Structure and water uptake in $\text{BaLnCo}_2\text{O}_{6-\delta}$ (Ln = La, Pr, Nd, Sm, Gd, Tb and Dy) Acta Materialia, 199, 297-310, 2020
- 132 Wan, W., Triana, C.A., Lan, J., Li, J., Allen, C.S., Zhao, Y., Iannuzzi, M., Patzke, G.R. Bifunctional Single Atom Electrocatalysts: Coordination–Performance Correlations and Reaction Pathways ACS Nano, 14, 13279-13293, 2020
- 133 Wharmby, M.T., Niekel, F., Benecke, J., Waitschat, S., Reinsch, H., Daisenberger, D., Stock, N., Yot, P.G. Influence of Thermal and Mechanical Stimuli on the Behavior of Al-CAU-13 Metal–Organic Framework Nanomaterials, 10, 1698, 2020
- 134 Werker, M., Ruschewitz, U. $\text{Cs}_2\text{Zn}(\text{CN})_4$: a first example of a non-cyano spinel of composition $\text{A}_2\text{M}(\text{CN})_4$ with A=alkali metal and M=group 12 metal Zeitschrift für Naturforschung B, in press, 2020
- 135 Yusenko, K.V., Martynova, S.A., Khandarkhaeva, S., Fedotenko, T., Glazyrin, K., Koemets, E., Bykov, M., Hanfland, M., Siemensmeyer, K., Smekhova, A., Gromilov, S.A., Dubrovinsky, L.S. High compressibility of synthetic analogous of binary iridium–ruthenium and ternary iridium–osmium–ruthenium minerals Materialia, 14, 100920, 2020
- 136 Zabilskiy, M., Sushkevich, V.L., Palagin, D., Newton, M.A., Krumeich, F., Van Bokhoven, J.A. The unique interplay between copper and zinc during catalytic carbon dioxide hydrogenation to methanol Nat. Commun., 11, 2409, 2020
- 137 Zacharakis, E., Bremmer, G.M., Vajeeston, P., Kalyva, M., Fjellvåg, H., Kooyman, P.J., Sjøstad, A.O. One-pot synthesis of cobalt–rhenium nanoparticles taking the unusual β -Mn type structure Nanoscale Adv., 2, 1850-1853, 2020
- 138 Zakharkin, M.V., Drozhzhin, O.A., Ryazantsev, S.V., Chernyshov, D., Kirsanova, M.A., Mikheev, I.V., Pazhetnov, E.M., Antipov, E.V., Stevenson, K.J. Electrochemical properties and evolution of the phase transformation behavior in the NASICON-type $\text{Na}_{3+x}\text{Mn}_x\text{V}_{2-x}(\text{PO}_4)_3$ ($0 \leq x \leq 1$) cathodes for Na-ion batteries J. Power Sources, 470, 228231, 2020
- 139 Zhang, Y., Tirani, F.F., Pattison, P., Schenk-Joß, K., Xiao, Z., Nazeeruddin, M.K., Gao, P. Zero-dimensional hybrid iodobismuthate derivatives: from structure study to photovoltaic application Dalton Trans., 49, 5815-5822, 2020
- 140 Zhao, Y., Mavrokefalos, K.C., Zhang, P., Erni, R., Li, J., Triana, A.C., Patzke, R.G. Self-Templating Strategies for Transition Metal Sulfide Nanoboxes as Robust Bifunctional Electrocatalysts Chem. Mater., 32, 4, 1371-1383, 2020
- 141 Zhou, Y., Zhou, H., Deng, J., Cha, W., Cai, Z. Decisive Structural and Functional Characterization of Halide Perovskites with Synchrotron Matter, 2, 360-377, 2020
- 142 Zucha, W., Weibel, G., Wolfers, M., Eggenberger, U. Inventory of MSWI Fly Ash in Switzerland: Heavy Metal Recovery Potential and Their Properties for Acid Leaching Processes, 8, 1668, 2020

Summary of the works

The ESRF has started to operate its beamlines with the new Extremely Brilliant Source in 2020. The SNBL has been preparing since 2017 for this event following a plan outlined in the “SNBL 2019-2020 and beyond” document. This document was supported by the Swiss- and Norwegian users, their respective steering committees and approved by the SNX Council. This document was sent out by PSI for international review and received excellent evaluations. The SNBL international beamline review panel in 2019 also strongly endorsed the project. The document was additionally handed over to the funding agencies in both Norway and Switzerland (RCN and SERI) in 2018.

In brief, the new EBS source provides excellent opportunities for SNBL users. In order to materialize these opportunities, a 2-phase plan for SNBL was therefore developed and consequently approved to adapt and upgrade both beamlines to the new EBS source. *Phase 1 covers investments in beamline equipment that are directly induced by the new source characteristics of the ESRF-EBS upgrade (i.e. higher heat load on the optical components).* Phase 2 provides an evolving scientific case for both BM01 and BM31 and their proof of concept. Obviously, the equipment installed now for Phase 1 is already compatible with the future scientific goals of the Phase 2 upgrade. According to this plan 2020 is fully targeted towards bringing the phase 1 upgrade to a good end. In 2020 the works at SNBL have therefore been focused on finalizing the phase 1 installations started in 2019, on commissioning the beamlines with the new EBS source and on a reliable and rapid restart of the user programs. Phase 2 is foreseen beyond 2020.

The planning of the three targets, 1) finishing installations, 2) commissioning with EBS and 3) restarting of the user program was severely influenced by the Covid 19 outbreak and subsequent lockdown's notably in the spring of 2020. Regardless of the pandemic all objectives have nevertheless been reached in 2020.

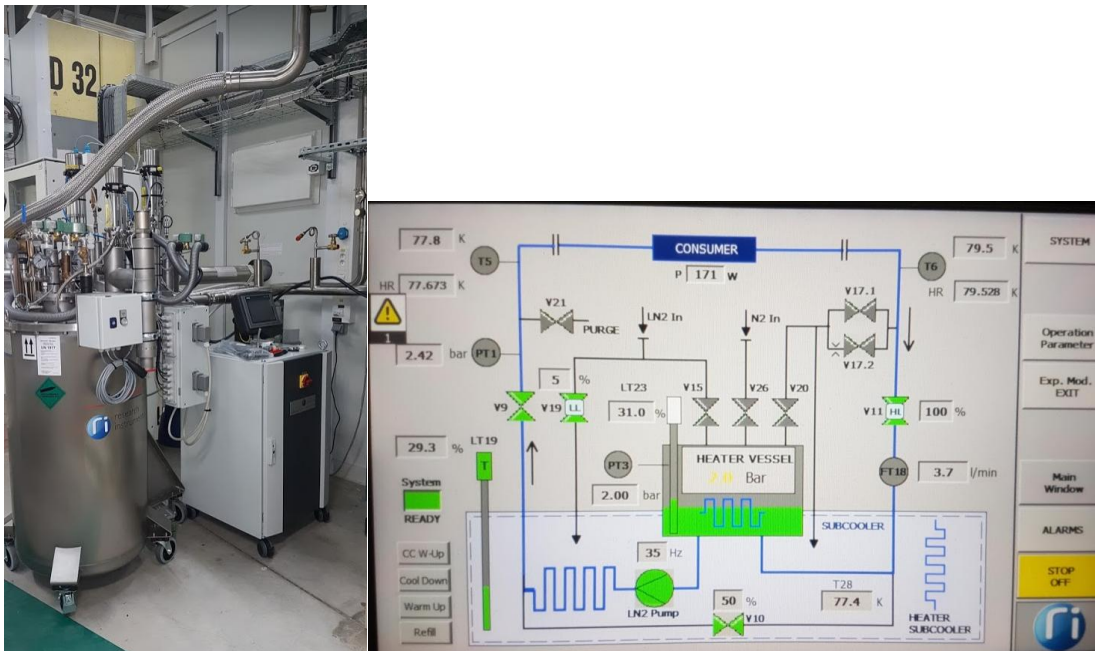
The BM01 phase 1 upgrade, consisting of a beamline move and vacuum conditioning, was ready before the originally planned first EBS beams in April 2020.



Newly installed monochromator on BM31

The phase 1 for BM31 mainly focussed on the installation of a new cryogenically cooled monochromator. This has been a major project needing large developments and human resources, in i.e. project

management, installation, alignment, controls, cabling, LN2 infrastructure and software. Most works were successfully performed in 2019, the major item for 2020 was the cryogenic circulator still to be delivered. Due to Covid19, this device came much later than originally planned but just in time for the new EBS restart date in July 2020.



Newly installed cryocooler and its operation display on BM31

The original restart and commissioning of the beamlines was planned for April 2020. This was delayed to mid-July 2020 when both SNBL beamlines were finally certified for its radiation safety under EBS conditions. This left only 9 days of commissioning before the summer shutdown.

The commissioning restarted on the 25th of August 2020 on both SNBL beamlines. The user program was restarted on BM01 as soon as September 9 2020. Nine official user experiments were planned on BM01 and successfully performed in 2020 in full remote mode, i.e. without on-site users due to Covid-19. Further beamline commissioning was performed in-between experiments from time to time. All experimental functionalities, powder, single crystal and surface diffraction are tested and operational.

The challenge and amount of commissioning work on BM31 was obviously much larger compared to BM01 as a completely new monochromator with multiple functionalities was installed. Several so-called “friendly” users’ experiments were performed before the first official user experiment on October 27 2020. Altogether four official users’ experiments could be planned and successfully performed in 2020. One external user could even come on-site in a gap in the continuously changing Covid-19 restrictions. Some mechanical interventions had to be made both inside the new monochromator and even inside the storage ring to bring the BM31 performance up to the projected level. At the end of the year the forecasted performance of the phase 1 upgrade was fully reached. In-situ and operando combined absorption and scattering experiments were performed. The now proven accuracy, precision, reproducibility and stability of the beamline and monochromator are according to specifications enabling combined XRD-XAFS-PDF foreseen in phase 2.